Reconstruction of bacterial transcription-coupled repair at single-molecule resolution

Jun Fan[1], Mathieu Leroux-Coyau[1], Nigel J. Savery[2], and Terence R. Strick[1,3,4]

[1]Institut Jacques Monod, CNRS, UMR7592, University Paris Diderot, Sorbonne Paris Cité F-75205 Paris, France

[2]DNA-Protein Interactions Unit, School of Biochemistry, University of Bristol, Bristol BS8 1 TD, UK

[3]Ecole Normale Supérieure, Institut de Biologie de l'Ecole Normale Superieure (IBENS), CNRS, INSERM, PSL Research University, 75005 Paris, France

[4]Programme Equipe Labellisées, Ligue Contre le Cancer, 75013 Paris, France

E. coli Mfd translocase enables transcription-coupled repair (TCR) by displacing RNA polymerase (RNAP) stalled on a DNA lesion and then coordinating assembly of the UvrAB(C) components at the damage site [1, 2, 3, 4]. Recent studies have shown that after binding to and dislodging stalled RNAP, Mfd remains on the DNA in the form of a stable, slowly translocating complex with evicted RNAP attached [5, 6]. Using a series of single-molecule assays, we find that recruitment of UvrA and UvrAB to Mfd-RNAP arrests the translocating complex and causes its dissolution. Correlative single-molecule nanomanipulation and fluorescence measurements show that dissolution of the complex leads to loss of both RNAP and Mfd. Subsequent DNA incision by UvrC is faster than when only UvrAB(C) are available, in part because UvrAB binds twenty- to two hundred times more strongly to Mfd-RNAP than to DNA damage. These observations provide a quantitative framework for comparison of complementary DNA repair pathways *in vivo*.

The conformational changes which take place in Mfd upon docking to, and activation by, stalled RNAP [7, 8, 9] enable it to bind to DNA upstream of RNAP and translocate along DNA against stalled RNAP [10, 11], and to expose a UvrB homology module and recruit UvrA [3]. Remarkably, single-molecule assays have shown that after displacing stalled RNAP to make the lesion accessible for repair, Mfd continues to translocate slowly and processively with RNAP attached to it [5, 6]. These assays help explain recent results showing that TCR can also accelerate repair of damaged sites downstream of the stall site [12]. Nevertheless, the role of the translocating Mfd-RNAP complex in stimulating repair by UvrAB(C) remains unclear. Here three single-molecule assays based on magnetic trapping [13] are brought to bear on the system.

In the tethered-RNAP translocation assay we stall biotinylated RNAP after transcribing twenty bases using only ATP, UTP and GTP on a DNA cassette that lacks C residues. We then tether the RNAP to a streptavidin-coated magnetic bead, and anchor the linear DNA template at one end to a modified glass coverslip. We thus obtain an RNAP stalled ~1 kbp from one end of an ~8 kbp DNA as it transcribes towards the distant glass surface [14] (Figure 1A). The DNA is extended away from the surface by a vertical force (F = 1 picoNewton, or pN) applied to the bead using a pair of magnets located above the sample, and the bead's position above the surface is detected in real-time using computer-aided videomicroscopy. Addition of 100 nM Mfd and 2 mM ATP causes motion of the bead towards the surface as an Mfd-RNAP complex forms and translocates along the DNA (Fig. 1B) [5, 6]. The complex is Michaelian with respect to ATP, with V_{max}^{ATP} = 4.7 ± 0.1 bp/s (SEM) and K_M^{ATP} = 16 ± 0.4 μM (SEM) (Extended Data Figure 1). In ~50% of cases the bead translocates ~7000 bp under the action of Mfd and is released only upon collision with the surface, in the remaining cases it releases prior to reaching the surface (Table 1).

Addition of 50 pM UvrA to translocating Mfd-RNAP (Fig. 1B) leads to release of 75% of beads prior to reaching the surface (Table 1). In 50% of release events we observe arrest of the translocating complex prior to release (65/132, see Table 1). Arrest duration is well-described by single-exponential kinetics with a mean duration of 15 +/- 3 s (SEM, see Fig. 1C). Accordingly, arrest most likely occurs in the remaining 50% of events but is too short for us to detect with a slow measurement response time of ~10 s (see Supplementary Information: Methods). Addition of 50 pM UvrA and 250 nM UvrB to the translocating complex leads to release of 93% of beads (Fig. 1B and Table 1). Arrest now lasts on average only 6 +/- 1 s (SEM, see Fig. 1D), and is observed in only ~20% of cases (Table 1). As above, shorter periods of arrest are predicted to have taken place in all cases. UvrB alone fails to destabilize the translocating complex (Fig. 1B and Table 1). ATP hydrolysis is required for either UvrA or UvrAB to carry out these tasks (Extended Data Fig. 2A, C). These results

indicate that complex resolution by UvrAB is faster and more efficient than by UvrA alone, and that arrest of the complex is on-pathway to its disassembly.

We next use a tethered-DNA assay in which a 2 kbp subfragment of the DNA used previously is attached to a magnetic bead and a coverslip, and extended (F=0.3 pN) and supercoiled in the magnetic trap (Fig. 2A) [13, 15]. In Fig. 2B we show the extension signal obtained when RNAP initiates transcription and stalls on a positively-supercoiled DNA substrate bearing a CPD, and is displaced by Mfd to form the long-lived translocating complex (denoted Intermediate, I, see Fig. 2B, Extended Data Fig. 3, 4 and [5]). Intermediate lifetimes are long and normally distributed (mean of 548 +/- 37s SEM) and are independent of supercoiling or cause of stalling (Extended Data Fig. 3) but depend on the distance between stalled RNAP and the end of the DNA (Extended Data Fig. 4). Addition of 50 pM UvrA and 250 nM UvrB reduces the mean lifetime of the Mfd-RNAP repair intermediate (Fig. 2C) to 141 ± 20s (SEM) in a manner that is essentially unaffected by supercoiling and cause of stalling (Extended Data Figs. 4 and 5). The lifetime distribution of the intermediate species now follows a difference-of-exponentials function characteristic of a Michaelis-Menten process with association/dissociation of UvrAB to translocating Mfd-RNAP (rates k_1 and k_{-1} respectively) and a slow forward catalytic rate for resolution of the complex k_2 (see model Fig. 4).

By titrating UvrA from 50 to 100 pM against a saturating concentration of 250 nM UvrB, we observe a gradual reduction in the mean lifetime of the Mfd-RNAP-DNA complex as expected for a diffusion-limited process (see Fig. 2D, Extended Data Fig. 6). By determining the mean lifetimes of intermediates for different UvrA concentrations and fitting those average values to a Michaelis-Menten model, we obtain K_M^{UvrAB} = 96 ± 51 pM (SEM) and V_{max}^{UvrAB} = 0.023 ± 0.006 s^{-1} ($1/V_{max}^{UvrAB}$ = 43 ± 12 s SEM) for dissolution of the Mfd-RNAP complex by UvrAB (Fig. 2D). By globally fitting the full lifetime distributions of Mfd-RNAP intermediates obtained at different UvrA concentrations to the single-molecule limit for the Michaelis-Menten equation [16], using the maximum velocity obtained above as a global constraint (Extended Data Fig. 6 and Supp. Info.), we estimate the on- and off-rates of the UvrAB complex with respect to the Mfd-RNAP intermediate as k_1 = 7.3 ± 1.9 × 10^8 M^{-1} s^{-1}, and k_{-1} = 0.037 ± 0.013 s^{-1}, giving a K_M^{UvrAB} of about 80 pM, in agreement with the estimate from average values. Control experiments show that removing Mfd, ATP, or UvrA abolishes complex dissolution (Extended Data Fig. 7). UvrB could not be removed however as UvrA, on its own, compacts DNA in a non-specific manner at concentrations as low as 10 pM, precluding its analysis unbuffered by UvrB in this assay (Extended Data Fig. 8). Importantly, DNA compaction by 100 pM UvrA is abolished by addition of 250 nM UvrB (Extended Data Fig. 8).

To further determine the fate of the Mfd-RNAP complex upon arrest and dissolution by UvrAB we use NanoCOSM [6], a recently developed assay enabling correlative nanomanipulation and

fluorescence colocalization of single-molecules. By tracking the Mfd-RNAP intermediate via its mechanical signature on DNA as seen in the topological assay, and simultaneously using single-molecule fluorescence to identify the colocalization of labelled components, we can monitor the composition of the repair complex as it progresses through TCR. Fluorescently-labelled RNAP appears in the fluorescence channel when transcription initiation is observed nanomechanically and is lost from that channel upon nanomechanical dissolution by UvrAB of the repair intermediate (Fig. 3A and Extended Data Fig. 9A). Similarly, fluorescently labelled Mfd appears in the fluorescence channel upon formation of the repair intermediate, and is lost from that channel upon dissolution by UvrAB of the repair intermediate (Fig. 3B and Extended Data Fig. 9B). Thus dissolution of the stable Mfd-RNAP intermediate by UvrAB involves loss of both Mfd and RNAP, indicating they do not act in downstream steps of DNA repair.

We finally used the tethered-DNA assay to measure TCR incision rates. DNA incision results in an abrupt loss of supercoiling and is readily detectable as a sudden increase in end-to-end extension. TCR incision is obtained by first stalling RNAP on a CPD, then pre-equilibrating the cell with UvrAB(C), and then rapidly adding Mfd to the system (see Fig. 3C). We measure $t_{incision}$, the time elapsed between remodeling of stalled RNAP by Mfd and DNA incision by UvrC. Incision times for positively and negatively supercoiled DNA follow single-exponential distributions with mean lifetimes of 380 ± 120 s (SEM, n=44 events) and 390 ± 70 s (SEM, n=59 events), respectively (Fig. 3D, E). This is significantly faster than incision rates of the CPD substrate in the presence of only UvrABC as in the case of global genome repair, or GGR (1230 ± 195 s, SEM, n=72 and 1156 ± 256 s, SEM, n=40 for positive and negative supercoiling, respectively; see Fig. 3F, G and Extended Data Fig. 10 for experiments and controls removing ATP, UvrAB, the CPD, or in which CPD is protected by RNAP). Our observation of an enhanced repair rate in this assay is consistent with prior biochemical findings [17, 12]].

TCR differs from GGR in the mode of recruitment of UvrAB to the lesion. UvrAB on its own displays reasonable affinity for DNA damage (dissociation constant in the 1-10 nM range [18]). Here we have shown that the dissociation constant of UvrAB from the activated Mfd-RNAP complex is twenty to two-hundred times smaller (k_{-1}/k_1 = 50 pM). This is partly due to the extremely efficient docking of UvrAB to the exposed UvrB homology module of the Mfd-RNAP complex ($k_1 \sim 7 \times 10^8$/M·s, essentially diffusion-limited). This efficiency can be explained by the fact that the UvrB homology module is larger and more accessible and thus easier to "find" than DNA damage. In this manner GGR components may actively participate in repair even in uninduced, non-SOS conditions, where abundance of UvrA is extremely low – in the 20 nM range, i.e. only about ten dimers per cell [19, 20] – and therefore also subject to large fluctuations. The TCR pathway we detail therefore appears to be

most relevant to “housekeeping” DNA repair, watchfully maintaining genomic integrity even in the absence of stressful or genotoxic conditions.

Our observations suggest the existence of a transient UvrB-UvrA-UvrA-Mfd-RNAP repair complex, which would convert into an UvrB-UvrA-UvrA complex after loss of Mfd and RNAP. Intriguingly, this complex is able to drive repair only of the transcribed strand of DNA – the hallmark of TCR [12]. This suggests the complex, once loaded onto the DNA, does not “pick up” a second UvrB. The single-molecule methods used here not only provide us with both broad and detailed views of TCR, but also provide us with the opportunity to pursue these advanced mechanistic questions.

Acknowledgements This work was made possible by a China Scholarship Council award to JF, as well as grants from the French Agence Nationale pour la Recherche (RepOne), and the European Science Foundation (EURYI) to TRS, as well as core funding from the CNRS and the University of Paris Diderot. The Strick lab is also part of the Programme Equipe Labellisées of the Ligue Contre le Cancer. We thank Nicolas Joly (Institut Jacques Monod, CNRS) for assistance with protein purification and the Strick laboratory for critical feedback.

The authors declare no competing financial interests.

Correspondence and requests for materials should be addressed to: strick@biologie.ens.fr

Contribution Statement JF, MLC, NJS and TRS planned out experiments; JF, MLC, and TRS prepared reagents; JF carried out tethered-RNAP, tethered-DNA, and NanoCOSM assays; MLC and TRS carried out tethered-RNAP assays. JF, MLC and TRS conducted data analysis, and NJS and TRS wrote the paper.

References

[1] E. M. Witkin. Radiation-induced mutations and their repair. *Science*, 152(3727):1345–1353, Jun 1966.

[2] I. Mellon, G. Spivak, and P.C. Hanawalt. Selective removal of transcription-blocking DNA damage from the transcribed strand of the mammalian DHFR gene. *Cell*, 51(2):241–249, Oct 1987.

[3] C.P. Selby and A. Sancar. Molecular mechanism of transcription-repair coupling. *Science*, 260(5104):53–58, Apr 1993.

[4] N.J. Savery. The molecular mechanism of transcription-coupled DNA repair. *Trends Microbiol.*, 15(7):326–333, Jul 2007.

[5] K. Howan, A.J. Smith, L.F. Westblade, N. Joly, W. Grange, S. Zorman, S.A. Darst, N.J. Savery, and T.R. Strick. Initiation of transcription-coupled repair characterized at single-molecule resolution. *Nature*, 490(7420):431–434, Oct 2012.

[6] E.T. Graves, C. Duboc, J. Fan, F. Stransky, M. Leroux-Coyau, and T.R Strick. A dynamic dna-repair complex observed by correlative single-molecule nanomanipulation and fluorescence. *Nat. Struct. Mol. Biol.*, 22:452–457, 2015.

[7] A.M. Deaconescu, A.L. Chambers, A.J. Smith, B.E. Nickels, A. Hochschild, N.J. Savery, and S.A. Darst. Structural basis for bacterial transcription-coupled DNA repair. *Cell*, 124(3):507–520, Feb 2006.

[8] L.F. Westblade, E.A. Campbell, C. Pukhrambam, J.C. Padovan, B.E. Nickels, V. Lamour, and S.A. Darst. Structural basis for the bacterial transcription-repair coupling factor/RNA polymerase interaction. *Nucleic Acids Res.*, 38(22):8357–8369, Dec 2010.

[9] D.B. Srivastava and S.A. Darst. Derepression of bacterial transcription-repair coupling factor is associated with a profound conformational change. *J. Mol. Biol.*, 406(2):275–284, Feb 2011.

[10] J.-S. Park, M.T. Marr, and J.W. Roberts. E. coli Transcription repair coupling factor (Mfd protein) rescues arrested complexes by promoting forward translocation. *Cell*, 109(6):757–767, Jun 2002.

[11] A.J. Smith, M.D. Szczelkun, and N.J. Savery. Controlling the motor activity of a transcription-repair coupling factor: autoinhibition and the role of RNA polymerase. *Nucleic Acids Res.*, 35(6):1802–1811, 2007.

[12] N.M. Haines, Y.-I.T. Kim, A.J. Smith, and N.J. Savery. Stalled transcription complexes promote DNA repair at a distance. *Proc. Natl. Acad. Sci. (USA).*, 111(11):4037–4042, Mar 2014.

[13] T. Strick, J.F. Allemand, D. Bensimon, A. Bensimon, and V. Croquette. The elasticity of a single supercoiled DNA molecule. *Science*, 271:1835 –1837, 1996.

[14] M.D. Wang, M.J. Schnitzer, H. Yin, R. Landick, J. Gelles, and S. Block. Force and Velocity Measured for Single Molecules of RNA Polymerase. *Science*, 282:902–907, 1998.

[15] A. Revyakin, C.-Y. Liu, R.H. Ebright, and T.R. Strick. Abortive initiation and productive initiation by RNA polymerase involve DNA scrunching. *Science*, 314:1139–1143, 2006.

[16] S.C. Kou, B.J. Cherayil, W. Min, B.P. English, and X. Sunney Xie. Single-Molecule Michaelis-Menten Equations. *J. Phys. Chem. B*, 109:19068–19081, 2005.

[17] L. Manelyte, Y.-I.T. Kim, A.J. Smith, R.M. Smit, and N.J. Savery. Regulation and rate enhancement during transcription-coupled DNA repair. *Mol. Cell*, 40(5):714–724, Dec 2010.

[18] B. Van Houten, H. Gamper, A. Sancar, and J. E. Hearst. Dnase i footprint of abc excinuclease. *J Biol Chem*, 262(27):13180–13187, Sep 1987.

[19] C. P. Selby and A. Sancar. Structure and function of the (a)bc excinuclease of escherichia coli. *Mutat Res*, 236(2-3):203–211, 1990.

[20] Y. Taniguchi, P.J. Choi, G.-W. Li, H. Chen, M. Babu, J. Hearn, A. Emili, and X. Sunney Xie. Quantifying E. coli Proteome and Transcriptome with Single-Molecule Sensitivity in Single Cells. *Science*, 329(5991):533–538, Jul 2010.

[21] A. Revyakin, R.H. Ebright, and T.R. Strick. Promoter unwinding and promoter clearance by RNA polymerase: detection by single-molecule DNA nanomanipulation. *Proc. Natl. Acad. Sci (USA)*, 101:4776–4780, 2004.

	Dissociation prior to surface		Dissociation by surface collision	Efficiency of release
	Pausing detected	No pausing detected		
Mfd-RNAP alone		33	66	33%
+UvrA	65	67	43	75%
+UvrAB	63	208	20	93%
+UvrB	0	5	65	8%

Table 1 Statistics of release of the Mfd-RNAP complex in the translocation assay.

Figure Legends

Figure 1| Tethered-RNAP assay for resolution of the Mfd-RNAP complex. (**A**) UvrA(B) intercepts, arrests and releases translocating Mfd-RNAP-bead complexes (see text). (**B**) Time-traces of bead position in the presence of 2 mM ATP and proteins as indicated. Arrows indicate component infusion (gaps). (**C**) Single-exponential lifetime distribution of arrest events in the presence of UvrA displays a mean of 15±3s (SEM, n=65). Inset time-trace shows Mfd-RNAP arrest (black bar) and release (red uparrow) for 10s averaging. Dashed line: linear fit to translocation. (**D**) As in C but in the presence of UvrA and UvrB. Mean arrest time now 6±1s (SEM, n=77).

Figure 2| Tethered-DNA assay for resolution of the Mfd-RNAP complex. (**A**) Transcription complexes can be monitored as the positively supercoiled DNA couples local torsional deformation by RNAP into large-scale looping (writhe) deformation [21]. (**B**) (Left) Tethered-DNA time-trace from CPD-bearing DNA in the presence of RNAP, Mfd, GreB, UTP, GTP, CTP and 2 mM ATP shows formation of: initially transcribing complex (RPitc), stalled elongation complex (RDe), and Mfd-RNAP repair intermediate (I) which resolves to baseline. (Right) Lifetime of Intermediate follows a Gaussian distribution (red line; n=21). (**C**) As in (B) but adding UvrA and UvrB (n = 58). (Right) Red line is the predicted distribution based on kinetic constants (main text). **(D)** Intermediate lifetime plotted as a function of inverse concentration of UvrA, obtained as in (C) but for RNAP stalled on a positively-supercoiled C-less cassette.

Figure 3 | Correlative single-molecule analysis of Mfd-RNAP handoff to UvrAB, and downstream DNA incision by UvrC. Time-traces showing simultaneous tethered-DNA assay of Mfd-RNAP repair intermediate formation and resolution by UvrAB, and single-molecule fluorescence signals from experiments in which **(A)** RNAP (n=14) or **(B)** Mfd (n=21) were fluorescently-labelled (Fluo-RNAP or Fluo-Mfd [6]). The traces presented were obtained on C-less cassette DNA. **(C)** Tethered-DNA time-trace for the TCR incision assay carried out on positively supercoiled, CPD-bearing DNA. Downarrows: stall RNAP at lesion; preequilibrate with UvrA, UvrB, UvrC, pUC18 DNA, GreB and NTPs; add 100 nM Mfd and 1 mM ATP (see text and Supplementary Information). Incision time distribution and exponential fits for **(D, E)** TCR and **(F, G)** GGR on positively or negatively supercoiled CPD-containing DNA, respectively.

Figure 4 | A model for the TCR pathway Stalled RNAP recruits and activates Mfd (denoted Mfd*), which then displaces RNAP from the lesion. Upon displacement of stalled RNAP, Mfd* remains attached to RNAP and continues to slowly translocate along the DNA. Mfd* can in turn recruit UvrAB, leading to arrest and release of the Mfd-RNAP complex from DNA in an ATP-dependent manner. We propose that this places UvrAB in the immediate vicinity of the lesion, ultimately increasing the rate at which UvrAB finds the lesion. UvrB-DNA can then recruit UvrC, which incises the lesion site.

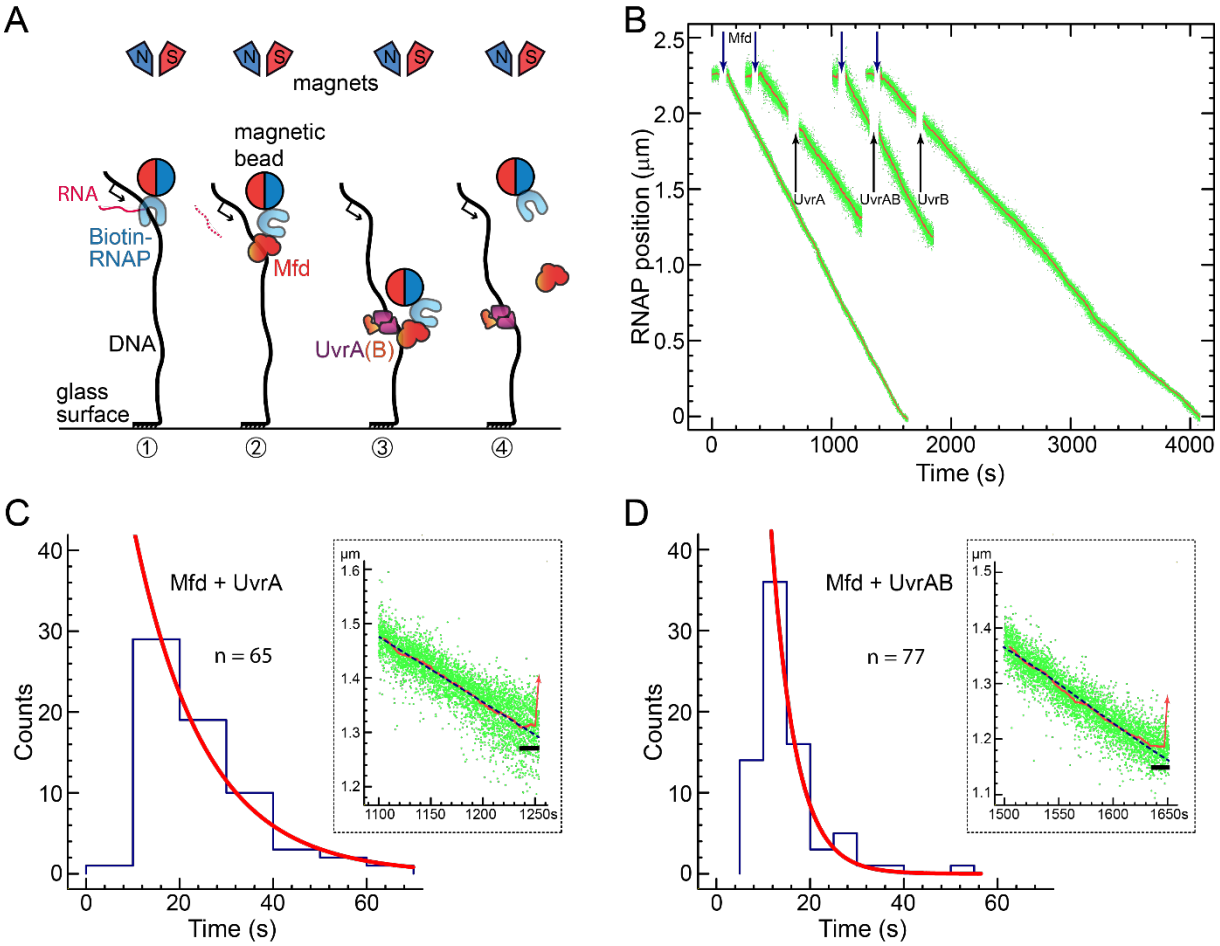
A
magnets
magnetic bead
RNA
Biotin-RNAP
Mfd
DNA
UvrA(B)
glass surface
①
②
③
④
B
Mfd
UvrA
UvrAB
UvrB
RNAP position (μm)
Time (s)
C
Mfd + UvrA
n = 65
Counts
Time (s)
μm
D
Mfd + UvrAB
n = 77
Counts
Time (s)
μm

Figure 1

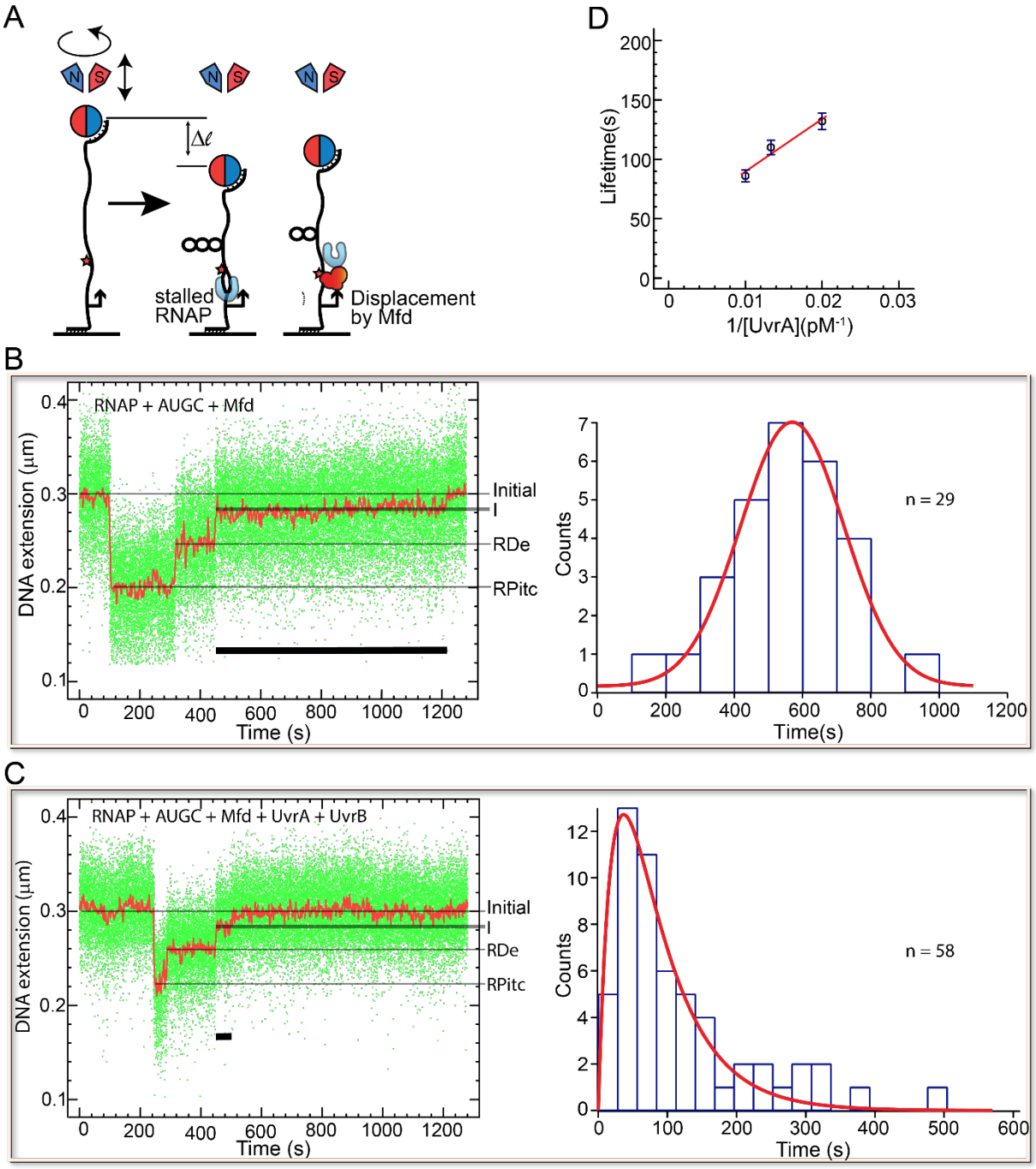
A
N
S
Δℓ
stalled
RNAP
Displacement
by Mfd
D
Lifetime(s)
1/[UvrA](pM-1)
B
RNAP + AUGC + Mfd
DNA extension (μm)
Time (s)
Initial
I
RDe
RPitc
Counts
n = 29
Time(s)
C
RNAP + AUGC + Mfd + UvrA + UvrB
DNA extension (μm)
Time (s)
Initial
I
RDe
RPitc
Counts
n = 58
Time (s)

Figure 2

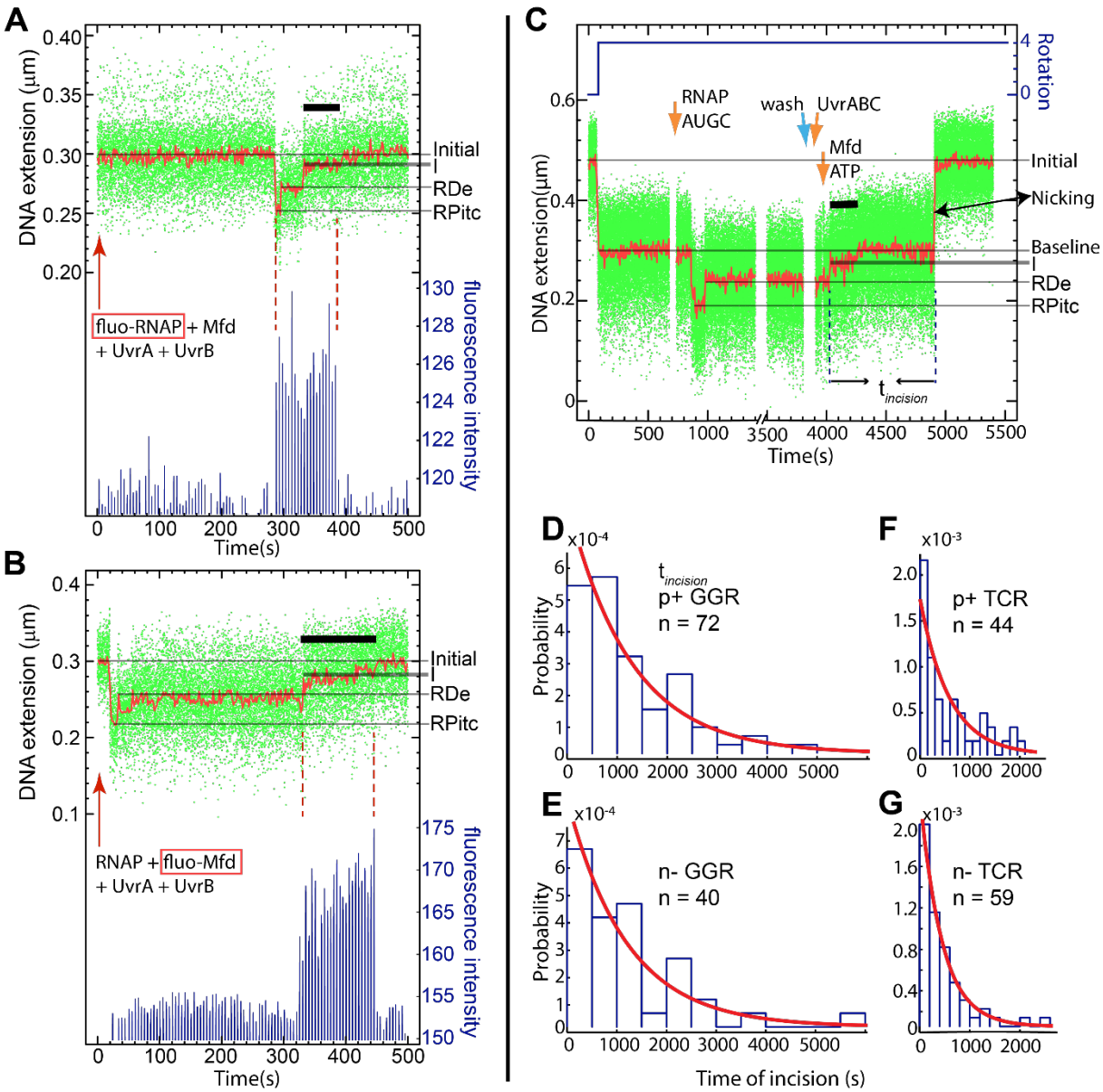
A
DNA extension (µm)
Initial
RDe
RPitc
fluo-RNAP + Mfd
+ UvrA + UvrB
fluorescence intensity
Time(s)
B
DNA extension (µm)
Initial
RDe
RPitc
RNAP + fluo-Mfd
+ UvrA + UvrB
fluorescence intensity
Time(s)
C
Rotation
RNAP
AUGC
wash
UvrABC
Mfd
ATP
Initial
Nicking
Baseline
RDe
RPitc
DNA extension(µm)
t incision
Time(s)
D
x10-4
t incision
p+ GGR
n = 72
Probability
F
x10-3
p+ TCR
n = 44
E
x10-4
n- GGR
n = 40
Probability
Time of incision (s)
G
x10-3
n- TCR
n = 59

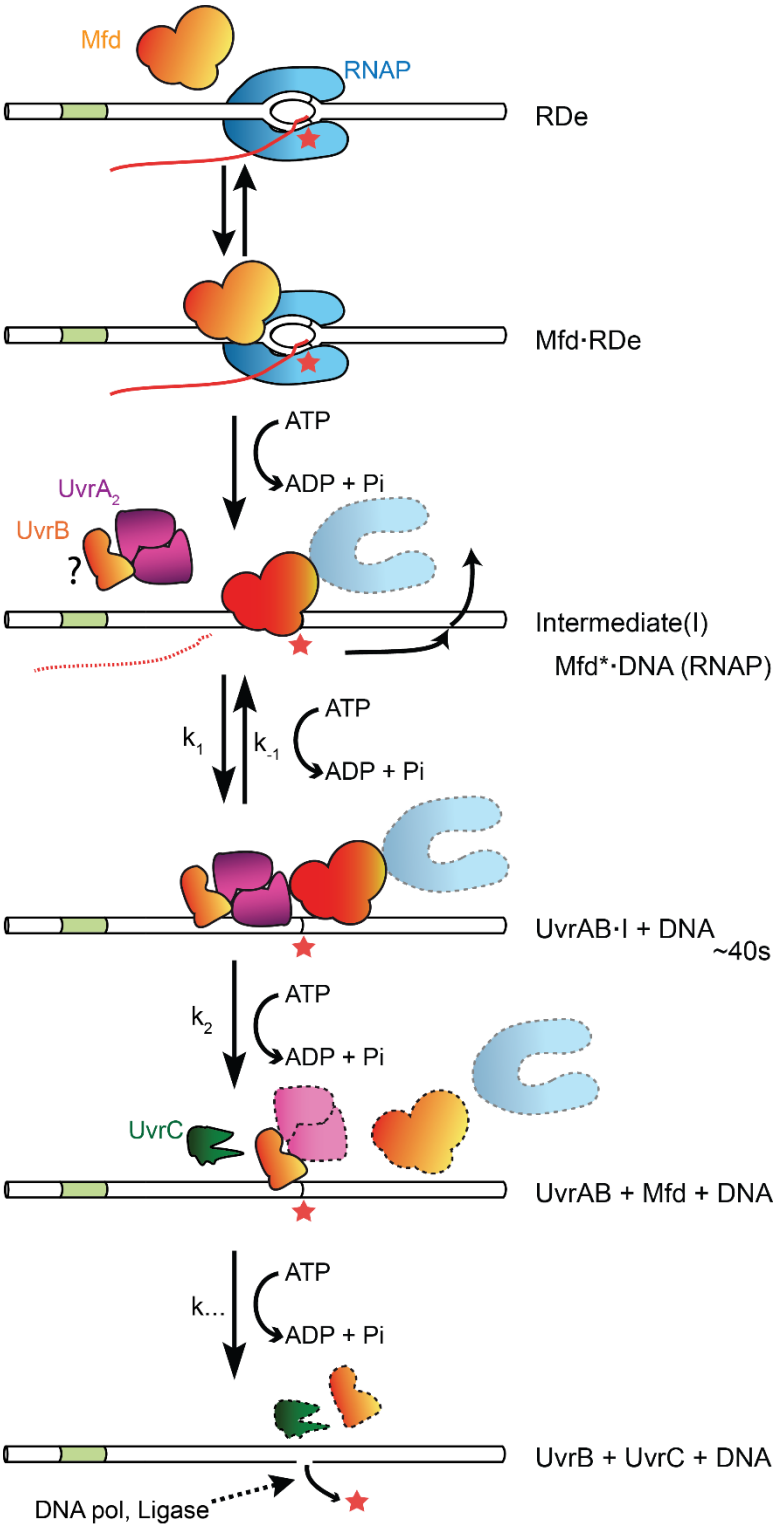
Mfd
RNAP
RDe
Mfd·RDe
ATP
ADP + Pi
UvrA2
UvrB
?
Intermediate(I)
Mfd*·DNA (RNAP)
k1
k-1
ATP
ADP + Pi
UvrAB·I + DNA
~40s
k2
ATP
ADP + Pi
UvrC
UvrAB + Mfd + DNA
k...
ATP
ADP + Pi
UvrB + UvrC + DNA
DNA pol, Ligase

Figure 4

Methods

DNA Constructs. Nanomanipulation constructs bearing the T5 N25 promoter [15] followed by either a C-less cassette (with the first C on the coding strand located at position +20 from the transcription start site, or TSS), or a CPD (at position +20 from the transcription start site, or TSS, and on the transcribed strand), were constructed as described previously [5, 6], but with one modification. Specifically, enzyme reactions used to prepare the constructs (restriction and ligation) were not heat-inactivated, but rather were purified of protein by use of a spin column for DNA purification (Macherey-Nagel). The transcription unit is:

5'TTGCTTTCAGGAAAATTTTTCTGTATAATAAGCTT**A**TAAATTTGAGAGAGGAGA**C**CAAATATGGCTGGTTCTC CACTAGTTCCGAATAG-3'

where the -35 and -10 promoter elements are underlined, the +1 TSS is in bold, and the first C on which RNAP stalls at +20 bold and underlined.

DNA nanomanipulation constructs used for tethered-RNAP translocation assays (as per Figure 1) were ~8 kbp long and contained the transcription unit at the DNA end distal to the surface and oriented in such a way as to direct initial transcription towards the surface [6].

DNA nanomanipulation constructs used for the tethered-DNA supercoiling assays (as per Figure 2) were all 2 kbp long and contained the transcription unit as a centrally-located cassette, except for experiments employing negatively supercoiled DNA bearing a C-less cassette, in which case a shortened, 1 kbp long DNA construct containing the transcription unit as a centrally-located cassette was used for its enhanced spatial resolution [24, 15, 5, 6].

DNA nanomanipulation constructs used for NanoCOSM assays (as per Figure 3) were all 3 kbp long and contained the transcription unit located ~400 bp from the coverslip surface and oriented so as to direct initial transcription towards the surface [6].

Proteins. *E. coli* RNAP, σ^{70}, GreB and Mfd, as well as SNAP-tagged RNAP (SNAP-RNAP) and SNAP-tagged Mfd (SNAP-Mfd) were purified as previously described [5, 6]. Core RNAP was saturated with a three-fold excess of σ^{70} to maintain polymerase in the holoenzyme form. SNAP-tagged proteins were labelled with BG-DY549 dye (New England Biolabs) as previously described [6]. UvrA, UvrB and UvrC proteins were purified via nickel-affinity chromatography as previously described [22], with the following modifications.

UvrA purified via nickel-affinity chromatography was then diluted six-fold with Heparin Buffer A (10 mM Tris·Cl pH 7.5, 50 mM KCl, 1 mM EDTA, 1 mM DTT, 5% glycerol) and loaded onto 10 ml of heparin resin (HiTrap Heparin, GE Healthcare) equilibrated in Heparin Buffer A. UvrA was eluted from the heparin resin by developing a gradient to 1 M KCl, concentrated as necessary to ~5 ml (10,000 MWCO Vivaspin 20, GE Healthcare) and then gel-filtrated (Superdex HiLoad 200 16/60, GE Healthcare) in GF Buffer (10 mM TrisCl pH 8, 200 mM KCl, 1 mM EDTA, 2 mM DTT, 5% glycerol) before overnight dialysis into GF Buffer containing 50% glycerol, aliquoting, and snap-freezing in LN_2.

UvrB purified via nickel-affinity chromatography was similarly diluted seven-fold with Heparin Buffer A to a conductivity of ~6 mS/cm before being loaded onto 10 ml of heparin resin equilibrated in Heparin Buffer A and eluted by developing a gradient to 1 M KCl. Peak fractions were diluted to a conductivity of ~6 mS/cm using Heparin Buffer A, loaded onto 1 ml of anion exchange resin (MonoQ 5/50 GL, GE Healthcare) equilibrated in Heparin Buffer A, and eluted by developing a gradient to 1 M KCl. Peak fractions were pooled and concentrated as necessary to ~5 ml (10,000 MWCO Vivaspin 20, GE

Healthcare) and then gel-filtrated (Superdex HiLoad 200 16/60, GE Healthcare) in GF Buffer before overnight dialysis into GF Buffer containing 50% glycerol, aliquoting and snap-freezing in LN_2.

UvrC purified via nickel-affinity chromatography was concentrated as necessary to ~5 ml (10,000 MWCO Vivaspin 20, GE Healthcare) and gel-filtrated (Superdex HiLoad 200 16/60, GE Healthcare) in GF Buffer UvrC (10 mM TrisCl pH 7.5, 350 mM KCl, 1 mM EDTA, 5% glycerol, 2 mM DTT) before overnight dialysis into GF Buffer UvrC containing 50% glycerol, aliquoting, and snap-freezing in LN_2.

Protein concentrations were determined using the Folin-Lowry assay. Protein preparations were free of non-specific nuclease activity as determined by the absence of incision of supercoiled plasmid DNA in overnight reactions at 37° C in standard repair buffer (RB, see below and [5, 6]) and in large excess of protein. The fully reconstituted UvrABC system was observed to specifically nick UV-irradiated plasmid DNA as expected.

Glass surfaces. Surfaces used in single-molecule nanomanipulation assays were derivatized with anti-digoxigenin [24], and surfaces used in correlative NanoCOSM assays were derivatized with streptavidin [6].

Reaction conditions. Experiments were performed at 34°C in buffer containing 40 mM K-Hepes pH 8.0, 100 mM KCl, 8 mM $MgCl_2$, 0.5 mg/ml BSA, 0.1 % w/v Tween 20, and 10 mM β-mercaptoethanol (adapted from [15, 23]). Unless specified otherwise, concentrations of components if present in reactions were: 10-25 pM RNAP holoenzyme, 50 pM UvrA, 250 nM UvrB, 100 pM UvrC, 100 pM pUC18 competitor DNA, 500 nM GreB, 100 nM Mfd, 2 mM ATP, and 200 μM each of UTP and GTP (for DNA bearing a C-less cassette) or 200 μM each of UTP, GTP and CTP (for DNA bearing a CPD). NanoCOSM assays were conducted at 27°C. Collecting the specified number of events, n, typically requires more than three experimental runs involving usually 5-20 DNA molecules simultaneously (technical replicates).

Nanomanipulation: formation of the Mfd-RNAP repair intermediate.

Tethered-RNAP assays

Tethered-RNAP translocation assays (as per Fig. 1) were carried out as described previously [6]. In these assays a biotinylated RNAP is loaded at one end of an ~8 kbp DNA construct using the T5 N25 promoter, and stalled using the C-less cassette located at +20 from the TSS. The stalled RNAP-DNA construct is then bound to the standard streptavidin-coated magnetic beads used in all these assays (MyOne Streptavidin C1, Life Technologies). When deposited on an anti-digoxigenin coated glass surface, the end of the ~8 kbp construct distal to the stalled RNAP, and which bears multiple digoxigenin groups, binds to the surface. The DNA is gently extended away from the surface using a low force (F = 1 picoNewton). Displacement of stalled RNAP and formation of the translocating Mfd-RNAP complex is initiated by adding Mfd (100 nM) and ATP (2 mM).

Tethered-DNA assays

Tethered-DNA nanomanipulation experiments (as per Fig. 2) were carried out according to the procedures detailed in [15, 21, 24, 25]. Standard reactions contained: extended, supercoiled DNA (F = 0.3 pN, superhelical density $\sigma = \pm 0.021$ for experiments using positive or negative supercoiled DNA, respectively), 10-25 pM RNAP holoenzyme, 500 nM GreB, 100 nM Mfd, and 2 mM ATP and 200 μM each of UTP and GTP (for DNA bearing a C-less cassette) or 2 mM ATP and 200 μM each of UTP, GTP and CTP (for DNA bearing a CPD).

Two methodologies – pulse-chase and continuous tracking – were used for these measurements. As previously shown [5, 15] the methodologies are absolutely equivalent in terms of quantitative analysis and simply represent optimizations of experiments which can have characteristically long or short timescales, respectively, as detailed below.

Pulse-chase Methodology

Single-round "pulse-chase" assays [5], in which a single RNAP is stalled on DNA before free components are washed out and downstream components are flowed in, are optimal for the observation of long-lived repair intermediates which must not be interrupted by reloading of a new RNAP molecule. Thus time-traces from pulse-chase experiments typically display a gap in the tracking data corresponding to the moment of component injection.

To stall RNAP on DNA we first injected 25 pM RNAP holoenzyme, 500 nM GreB and 200 μM nucleotides (ATP, UTP and GTP for experiments on DNA bearing a C-less cassette, and all four nucleotides for experiments on DNA bearing a CPD). Upon loading and stalling of RNAP, we wash out free RNAP holoenzyme while maintaining GreB and NTPs in solution. We then add 100 nM Mfd and 2 mM ATP to the reaction chamber to allow the reaction to begin with displacement of stalled RNAP.

This methodology was typically used to generate the quantitative kinetic data in which UvrAB are absent: Fig. 2B (time distribution) and Extended Data Figures 3, 7C. This methodology was also used to preload RNAP for TCR incision rate measurements presented Fig. 3C,D,E. in which case UvrA, UvrB and UvrC components were added as described below.

Continuous-tracking Methodology

Continuous tracking assays [5], in which all components are simultaneously present in solution, are optimal for the statistical observation of short-lived repair intermediates which are only rarely interrupted by reloading of a new RNAP molecule. Here we injected 10-25 pM RNAP holoenzyme, 500 nM GreB, 2 mM ATP and 200 μM nucleotides (UTP and GTP for experiments carried out using the C-less cassette, and UTP, GTP and CTP for experiments carried out using a CPD), and UvrA and UvrB as specified.

This methodology was typically used to generate uninterrupted time-traces for presentation purposes such as Fig. 2B, C (time traces) as well as the quantitative data shown in Fig. 2 C,D; Fig. 3 A,B; and Extended Data Figures 4, 5, 6 and 9.

NanoCOSM assays

NanoCOSM analysis is described in detail in [6]. Briefly, it is based on tethered-DNA experiments carried out using a magnetic trap microscope into which a total internal reflection (TIR), or evanescent, field has been introduced [26]. For these assays combining topological measurement on torsionally constrained DNA and single-molecule fluorescence, a slightly longer DNA backbone (3 kbp) is employed so as to prevent the autofluorescent bead from entering too much into the evanescent field used to excite the fluorophore label. The transcription cassette is unchanged. DNA superhelical density is held constant at $|\sigma| = 0.021$, but for this longer DNA this corresponds to +/- 6 turns of the DNA in the magnetic trap rather than +/- 4 employed for 2 kbp DNA substrates. In these experiments, one fluorescent component was tested at a time. When used, SNAP-RNAP was at 50 pM and SNAP-Mfd was at 2.5 nM. All components other than the fluorescent one were present at the same concentrations as for standard tethered-DNA assays described above, except for the fact that GreB was omitted and the bead and surface chemistries were inverted (i.e. streptavidin-modified glass surface and anti-digoxigenin coated magnetic bead [6]). NanoCOSM assays were carried out using the continuous-tracking methodology.

UvrABC (GGR) incision assay. Incision by UvrABC of positively or negatively supercoiled DNA bearing either a C-less cassette or a CPD was carried out in the presence of 1 nM UvrA, 250 nM UvrB, 100 pM UvrC, 2 mM ATP and 100 pM of competitor DNA (pUC18, used to reduce non-specific interactions between protein components and DNA).

Incision by UvrABC of positively supercoiled DNA bearing a CPD protected by a stalled RNAP was carried out by first stalling RNAP on nanomanipulated DNA (pulse-chase methodology as above) and then flowing in 1 nM UvrA, 250 nM UvrB, 100 pM UvrC, 2 mM ATP and 100 pM of competitor DNA.

Mfd-RNAP-UvrABC (TCR) incision assay. The TCR assay for positively or negatively supercoiled DNA bearing a CPD was performed using the single round pulse-chase methodology described above. First, we stalled RNAP on the CPD by equilibrating the reaction cell with 20 pM RNAP, 200 μM of each of the four nucleotides, and 500 nM GreB. We then washed out free components while maintaining GreB and NTPs in solution. We then supplemented the reaction chamber with 1 nM UvrA, 250 nM UvrB, 100 pM UvrC, 2 mM ATP and 100 pM pUC18 competitor DNA, and then further supplemented the reaction chamber with 100 nM Mfd to displace stalled RNAP and initiate the TCR reaction.

Data Acquisition and Analysis. Nanomanipulation data was collected on homebuilt magnetic traps running the Picotwist software suite for trap control and particle tracking and analysis (Picotwist S.A). Raw nanomanipulation data representing the magnetic bead position as observed under red illumination (650 nm) were collected at video rate (31 Hz, green points in time-traces) using a JAI CCD camera, and were filtered at ~1s for analysis (red line in time-traces). Fluorescence data colocalized to the magnetic beads was collected using the Solis software suite provided by the EMCCD manufacturer (Andor) under 532 nm strobed illumination conditions (0.5 s illumination every 5 s), and were synchronized to the nanomanipulation data using dedicated timing trigger pulses generated by the programmable counters of the CCD camera.

Interception of the Mfd-RNAP complex by UvrA and UvrAB and estimation of the fraction of arrest events too short to be observed.

To estimate the fraction of UvrA- or UvrAB-mediated Mfd-RNAP arrest events that are too short to observe, we first characterize the instrument response time. Thus the magnetic bead's vertical RMS fluctuations in the tethered-RNAP assay, where the extending force F ~ 1 pN, are ~15 nm. Given that the velocity of the Mfd-RNAP complex is only about 1.5 nm/s, we find an instrument response time of approximately 10 seconds. As events shorter than this may not be detectable, we estimate that the fraction of events which follow a single-exponential distribution with mean of 15 seconds, but have a duration shorter than 10 seconds, is of order 50%. Similarly, we estimate that the fraction of events which follow a single-exponential distribution with a mean of 6 seconds, but have a duration shorter than 10 seconds, is of order 80%. These values are in good agreement with observed fractions of missing arrest events, leading us to conclude that UvrA or UvrAB always arrest the translocating complex before dissociating it from the DNA.

[22] L. Manelyte, C.P. Guy, R.M. Smith, M.S. Dillingham, P. McGlynn, and N.J. Savery. The unstructured C-terminal extension of UvrD interacts with UvrB, but is dispensable for nucleotide excision repair. *DNA Repair (Amst)*, 8(11):1300–1310, Nov 2009.

[23] A.J. Smith and N.J. Savery. RNA polymerase mutants defective in the initiation of transcription-coupled DNA repair. *Nucleic Acids Res.*, 33:755–764, 2005.

[24] A. Revyakin, R.H. Ebright, and T.R. Strick. Single-molecule DNA nanomanipulation: improved resolution through use of shorter DNA fragments. *Nat. Methods*, 2(2):127–138, Feb 2005.

[25] A. Revyakin, J.F. Allemand, V. Croquette, R.H. Ebright, and T.R. Strick. Single-molecule DNA nanomanipulation: detection of promoter-unwinding events by RNA polymerase. *Methods Enzymol.*, 370:577–598, 2003.

[26] Camille Duboc, Evan T. Graves, and Terence R. Strick. Simple calibration of TIR field depth using the supercoiling response of DNA. *Methods*, Mar 2016.

Extended Data Figure Legends

Extended Data Figure 1. Motor properties of the translocating Mfd-RNAP complex as seen in the tethered-RNAP assay. (A) Velocity distribution of translocating Mfd-RNAP in the presence of 2 mM ATP and under a weak opposing load (F = 1 pN). Velocity is measured by fitting a single line segment to an entire translocation time-trace; this is made possible by the fact that velocity is essentially constant over the ~7000 bp of displacement which constitutes an entire trajectory. The velocity distribution is fit to a Gaussian, giving a mean velocity of 4.6 +/- 1 bp/s (SD; n=99 trajectories). **(B)** Tau plot of inverse velocity of translocating Mfd-RNAP as a function of inverse ATP concentration is well-fit to a line, indicating Michaelian behavior with K_M^{ATP} = 16 +/- 0.4 μM (SEM) and V_{max}^{ATP} = 4.7 +/- 0.1 bp/s (SEM). Error bars correspond to standard error on mean values as determined from at least ten trajectories for each ATP concentration.

Extended Data Figure 2. Resolution of the translocating Mfd-RNAP complex by UvrA or by UvrAB is ATP-dependent as shown by the tethered-RNAP translocation assay. Downarrows indicate addition of components as noted and as follows. Beginning with stalled RNAP, we add 100 nM Mfd and 2 mM ATP to form the translocating Mfd-RNAP complex. A wash step using 5 ml of reaction buffer lacking ATP is applied to remove (nearly) all the free ATP in solution, causing the translocating complex to come to a nearly complete halt. Then, **(A, B)** 50 pM UvrA or **(C, D)** 50 pM UvrA and 250 nM UvrB are added to the experiment. The complex is stable and release of the magnetic bead is not observed. Further addition of ATP-γ-S (2 mM, see panels C and D) does not permit bead release. However, final addition of ATP (2 mM) leads to rapid release. Red uparrows indicate bead release in panels C and D.

Extended Data Figure 3. Characterization of the long-lived Mfd-RNAP intermediate on 2 kb DNA using the tethered-DNA assay. (A, B) Nanomanipulation time-traces showing pulse-chase measurement of the lifetime of the Mfd-RNAP intermediate for CPD-bearing DNA under conditions of positive (+sc) and negative (-sc) supercoiling, respectively. Downarrows indicate moments of component addition as noted and as follows. First, we load RNAP onto DNA in standard conditions (25 pM RNAP holoenzyme, 500 nM GreB, and the appropriate nucleotide complement, each present at 200 μM). We then wash out free RNAP with reaction buffer supplemented with 500 nM GreB and the nucleotide complement. We then initiate formation of the intermediate by infusion of the above wash solution supplemented with 100 nM Mfd and 2 mM ATP. For negatively supercoiled DNA, RNAP was loaded under conditions of positive supercoiling before the DNA was returned to negative supercoiling; blue line indicates when DNA supercoiling is changed. Black bar highlights the intermediate state. **(C, D)** Lifetime distributions for the Mfd-RNAP intermediate formed on CPD-bearing DNA under conditions of positive or negative supercoiling, respectively, are well-fit to Gaussian distributions. For positive supercoiling the mean lifetime of the repair intermediate is 548 ± 37 s (SEM, n=29 events: this distribution is presented also in Fig. 2B), and for negative supercoiling the mean lifetime of the repair intermediate is 556 ± 33 s (SEM, n= 21 events). **(E, F)** Lifetime distributions for the Mfd-RNAP intermediate formed on C-less cassette DNA under conditions of positive or negative supercoiling, respectively, are also well-fit to Gaussian distributions. For positive supercoiling the mean lifetime of the repair intermediate is 649 ± 13 s (n=98 events) and for negative supercoiling the mean lifetime of the repair intermediate is 524 ± 26 s (n= 46 events).

Extended Data Figure 4. Characterization of the Mfd-RNAP intermediate on negatively supercoiled 1 kb DNA in the absence or presence of UvrAB using the tethered-DNA assay. DNA bears a C-less cassette. **(A)** Nanomanipulation time-trace obtained in continuous-tracking mode in the presence of 25 pM RNAP holoenzyme, 100 nM Mfd, 500 nM GreB, 2 mM ATP, 200 μM UTP and 200 μM GTP. **(B)** As in the prior panel but in the added presence of 50 pM UvrA and 250 nM UvrB. **(C)** Lifetime distribution of the Mfd-RNAP intermediate in the absence of UvrA and UvrB has a mean lifetime of 258

± 17 s (SEM, n=33 events). **(D)** Lifetime distribution of the Mfd-RNAP intermediate in the added presence of 50 pM UvrA and 250 nM UvrB has a mean lifetime of 167 ± 17 s (SEM, n=32 events). Datasets for kinetics were obtained using the pulse-chase methodology.

Extended Data Figure 5. Reduced lifetime of the Mfd-RNAP intermediate in the presence of UvrAB, monitored using the tethered-DNA assay. (A) Nanomanipulation time-trace for positively supercoiled DNA (+sc) bearing a C-less cassette in the presence of 25 pM RNAP holoenzyme, 100 nM Mfd, 50 pM UvrA, 250 nM UvrB, 500 nM GreB, 2 mM ATP, 200 μM UTP, and 200 μM GTP (continuous-tracking methodology). **(B)** Nanomanipulation time-trace obtained as in (A) but for negatively supercoiled DNA (-sc). **(C-F)** Lifetime distributions for the Mfd-RNAP intermediate in the presence of UvrA and UvrB as above are essentially independent of both the cause of RNAP stalling (either a C-less cassette or a CPD) and supercoiling of the DNA (positive or negative). For positively supercoiled template the mean lifetime observed using DNA bearing a C-less cassette is 132 ± 7 s (SEM, n = 210, panel **C**, see overview in Extended Data Fig. 6D) and for DNA bearing a CPD it is 141 ± 20s (SEM, n = 58, panel **E**). For negatively supercoiled template the mean lifetime observed using DNA bearing a C-less cassette is 132 ± 13 s (SEM, n = 65, panel **D**) and for DNA bearing a CPD it is 157 ± 65 s (SEM, n = 10, panel **F**).

Extended Data Figure 6. Lifetime distributions of the Mfd-RNAP intermediate as a function of UvrA concentration, using the tethered-DNA assay. The DNA substrate used in these experiments was positively supercoiled and contained a C-less cassette, and data were collected using the continuous-tracking methodology in the presence of 10-20 pM RNAP holoenzyme, 500 nM GreB, 100 nM Mfd, 2 mM ATP, 200 μM UTP, 200 μM GTP, and 250 nM UvrB. The UvrA concentration was **(A)** 50 pM, **(B)** 75 pM and **(C)** 100 pM. Red lines show the result of global fiting to a difference-of-two exponentials characteristic of a Michaelis-Menten process, using the rate-limiting forward catalytic step extracted from classical Michaelian analysis of the mean times (Fig. 2D) as an additional constraint. **(D)** Overview of lifetimes of the Mfd-RNAP complex measured with the tethered-DNA assay and as a function of template supercoiling, cause of RNAP stalling, and UvrA concentration, as presented in the manuscript. UvrB was fixed at 250 nM throughout.

Extended Data Figure 7. Mfd-RNAP-UvrAB control experiments, using the tethered-DNA assay. These experiments were carried out on positively supercoiled DNA substrate (+sc) bearing a C-less cassette and using the standard pulse-chase methodology. **(A) No ATP Control: ATP dependence of UvrAB remodeling of Mfd-RNAP intermediate.** Black downarrows indicate component infusion as follows. (RNAP) We first introduce 25 pM RNAP holoenzyme, 500 nM GreB, 200 μM ATP, 200 μM UTP, and 200 μM GTP, and wait for RNAP to stall on DNA. (Wash) We next wash out all free components except for GreB. (Mfd ATP) We next infuse 100 nM Mfd, 500 nM GreB, and 50 μM ATP and wait for Mfd to remodel RNAP and form the Mfd-RNAP intermediate. (Wash) We next wash out all free components except GreB. (UvrAB) We next infuse 50 pM UvrA, 250 nM UvrB and 500 nM GreB. We wait several thousand seconds, without any observed change in the intermediate state. (ATP) Finally, we infuse 2 mM ATP into the reaction and rapidly observe resolution of the intermediate species. **(B) No MFD Control: UvrAB does not functionally interact with RNAP in the absence of Mfd.** Stalled RNAP formed as in panel A is not displaced in the presence of (downarrow) 50 pM UvrA, 250 nM UvrB, 500 nM GreB and 2 mM ATP. **(C) No UvrA Control: Lifetime distribution for the Mfd-RNAP intermediate in the presence of UvrB alone.** Stalled RNAP is formed as in panel A. We then wash out free RNAP while maintaining GreB and NTPs in solution, and then add 100 nM Mfd, 250 nM UvrB, and 2 mM ATP while maintaining GreB and NTPs in solution. The lifetime of the Mfd-RNAP intermediate thus formed remains long-lived (642 ± 22 s SEM, n= 80) with Gaussian statistics.

Extended Data Figure 8. Control Experiments for UvrA and UvrB interactions with DNA in the absence of damage as seen in the tethered-DNA supercoiling assay. Experiments were conducted on

positively supercoiled DNA bearing a CTP-less cassette. **(A)** UvrA alone compacts undamaged DNA in a non-specific manner even at concentrations as low as 10 pM. Trace shown obtained with 1 mM ATP; the same phenomenon is observed in the absence of ATP (data not shown). **(B)** UvrB prevents non-specific interaction of UvrA with DNA. (t=0 s) 250 nM UvrB alone does not compact DNA, although it transiently interacts non-specifically and briefly with DNA in the presence of 1 mM ATP, (see C-F). The same phenomenon is observed in the absence of ATP (data not shown). (t=2000 s) Addition of UvrB also prevents UvrA from compacting DNA non-specifically. Based on these data we set the working UvrB concentration to 250 nM: our measurements with UvrA can thus go up to 100 pM, which remain more than 90% saturated by this concentration of UvrB as shown by the fact that we can carry out measurements without DNA compaction. (**C-D)** Time traces obtained on positively supercoiled DNA in the presence of 250 nM UvrB and 1 mM ATP show supercoiling-dependence of the dwell time (t_{dwell}) of UvrB-DNA "wrapping" events. Indeed the amplitude of these events (~50-100 nm) is consistent with titration of a large positive supercoil by formation of a tight/compact, positive wrap of DNA around UvrB as observed in AFM imaging [27]. **(E-F)** Histograms of the dwell time of the wrap state obtained above are fit to single-exponential distributions, with a mean dwell time of (E) 28 ± 2 s (SEM, n = 175, +5 turns), and (F) 66 ± 5 s (SEM, n = 117, +6 turns). By carrying out experiments with no more than 250 nM UvrB and with only +4 turns of positive supercoiling, this wrap state is of order 10 s and does not significantly interfere with detection of Mfd-RNAP intermediates or their resolution, and UvrB safely inhibits DNA compaction activity by UvrA.

Extended Data Figure 9. Correlation between resolution of the Mfd-RNAP intermediate and loss of fluorescent signal from labelled RNAP or Mfd in the NanoCOSM assay. We plot the time elapsed between loss of fluorescence signal from (**A**) fluorescent RNAP or (**B**) fluorescent Mfd and nanomechanical resolution of the Mfd-RNAP intermediate as observed in the magnetic trap, as shown in Fig. 3A,B. In both cases the vast majority of events are correlated as shown by the fact that loss of fluorescence and nanomechanical resolution of the intermediate temporally coincide (i.e. the time between the two events is nil). Loss of fluorescence prior to nanomechanical resolution (i.e. indicated as positive times) is most likely due to spontaneous photobleaching of the DY-549 fluorophore used to label proteins. No significant difference is observed between DNA substrates bearing a CPD or bearing a C-less cassette.

Extended Data Figure 10. Characterization of (A, B) specific, (C, D) control, and (E-G) nonspecific GGR incision using the tethered-DNA assay. (A-B) Time traces showing GGR incision on positively and negatively supercoiled CPD-bearing DNA. For positively supercoiled DNA (+sc), addition of UvrABC proteins (1nM UvrA, 250nM UvrB, 100pM UvrC, and 100 pM pUC18 competitor DNA) and 1 mM ATP, led to DNA incision and an abrupt loss of supercoiling. The average GGR incision times are 1230 ± 195s (SEM, n=72 events) and 1156 ± 256 s (SEM, n=40 events) for +sc and –sc, respectively; see Fig. 3F, G of the main text for distributions and fits. **(C)** As in A, but in the absence of ATP. The absence of incision was confirmed on 22 molecules over a ~4h window. Upon supplementing the reactions with 1 mM ATP (red downarrow) incision rapidly takes place. **(D)** 100 pM UvrC and 1 mM ATP are unable to incise positively-supercoiled, CPD-bearing DNA. The absence of incision was confirmed on 31 molecules over a ~2h window. **(E)** Incision times for UvrABC (as above) acting on positively supercoiled DNA bearing a C-less cassette (i.e., undamaged) are essentially normally distributed (red line) with a mean of 2922 ± 222 s (n=44 events; fit was obtained by excluding points between 3000 and 4000s). **(F)** Incision times for UvrABC (as above) acting on negatively supercoiled DNA bearing a C-less cassette are essentially normally distributed with a mean of 2471 ± 377 s (SEM, n=28 events; fit was obtained by excluding points below 1000s). **(G)** Incision times for UvrABC acting on positively supercoiled DNA bearing a CPD protected by stalled RNAP in the absence of Mfd are essentially normally distributed with a mean of 2348 ± 672 s (SEM, n=31 events). Red lines are guides to the eye. (C-D) and overall results confirm all of UvrAB, UvrC, and ATP are required for GGR incision. Results from (E-G) further indicate that nonspecific DNA incision by the complete GGR system can take in this assay, however it is slow enough as to permit measurement of faster specific incision rates discussed Fig. 3. We propose these incision

events are in fact specific to the multiple biotin- and digoxigenin-based tethers at the ends of the DNA construct which can ultimately be recognized as DNA damage by the GGR machinery [9]. Because only nicking at the first tethering biotin or dig, and *within* the 2 kbp fragment, will result in loss of supercoiling, then, statistically, multiple incisions at multiple tethers must be realized before loss of supercoiling, resulting in a normal distribution. This can be compared to DNA incision by endonuclease, the time distribution of which is single-exponential [28]. As incision on these constructs is significantly slower and obeys different statistics than that on CPD-containing DNA, we conclude that our single-molecule measurements can indeed isolate CPD-specific from non-specific incision by the GGR machinery.

Extended References

[27] E.E.A. Verhoeven, C. Wyman, G.F. Moolenaar, J.H.J. Hoeijmakers, and N. Goosen. Architecture of nucleotide excision repair complexes: DNA is wrapped by UvrB before and after damage recognition. *EMBO J.*, 20(3):601–611, Feb 2001.

[28] B. van den Broek, M.C. Noom, and G.J.L. Wuite. Dna-tension dependence of restriction enzyme activity reveals mechanochemical properties of the reaction pathway. *Nucleic Acids Res.*, 33(8):2676–2684, 2005.

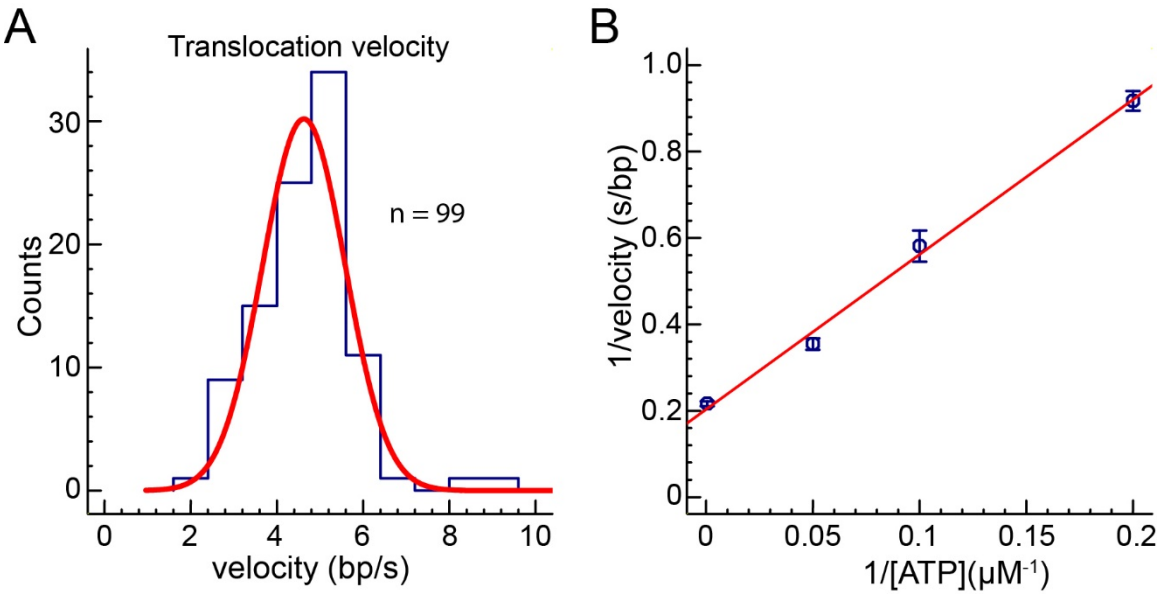

Extended Data Figure 1

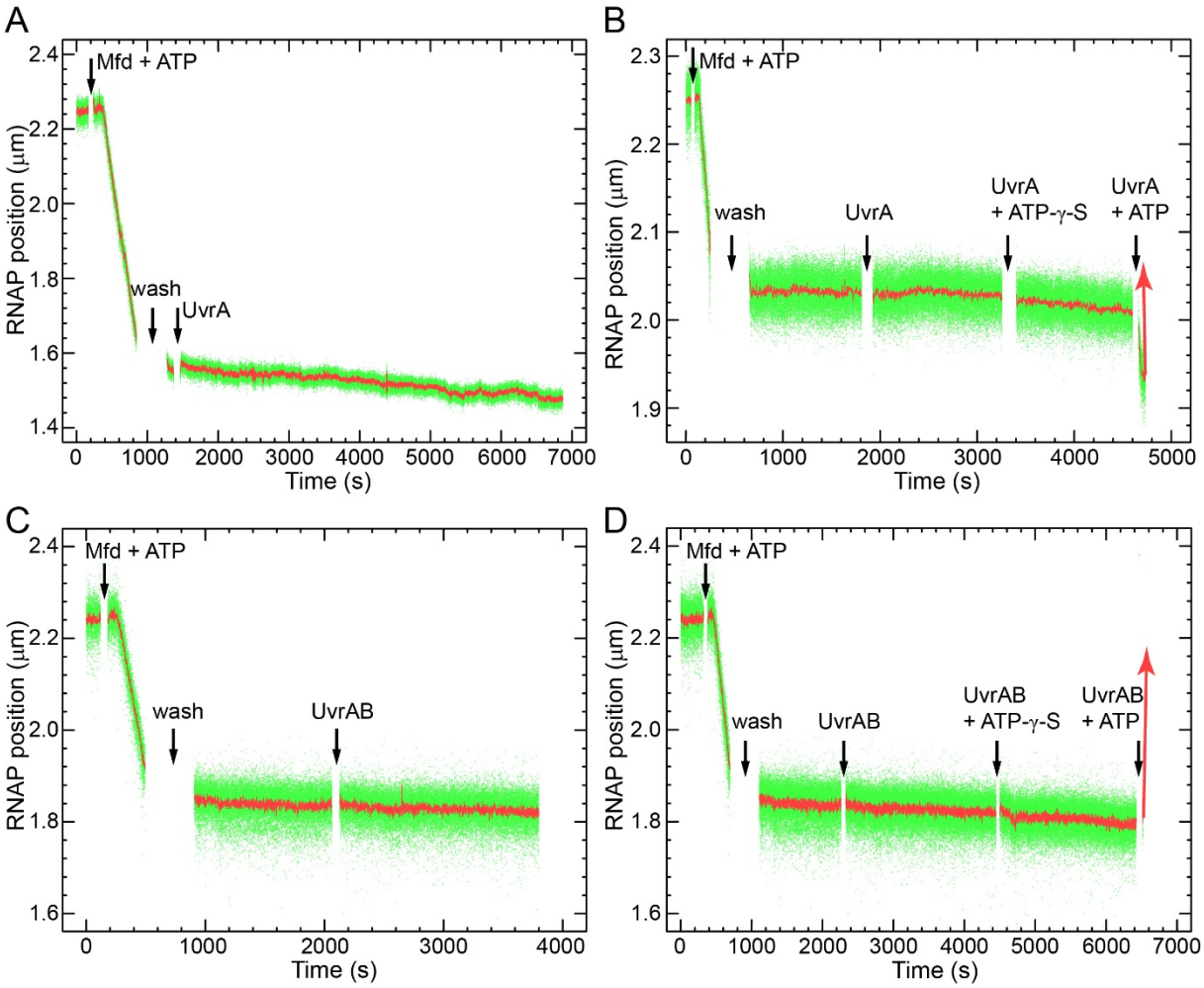

Extended Data Figure 2

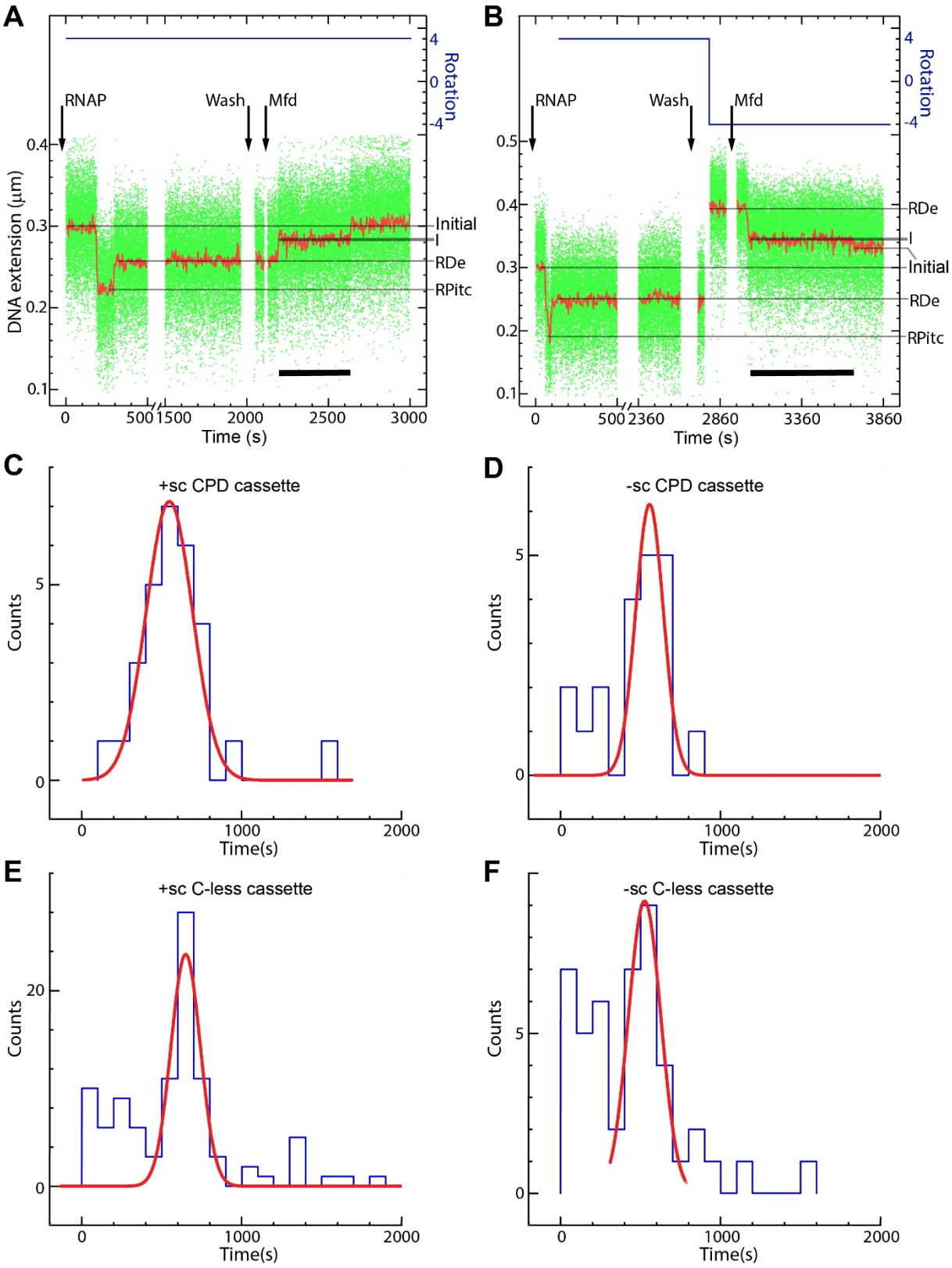

Extended Data Figure 3

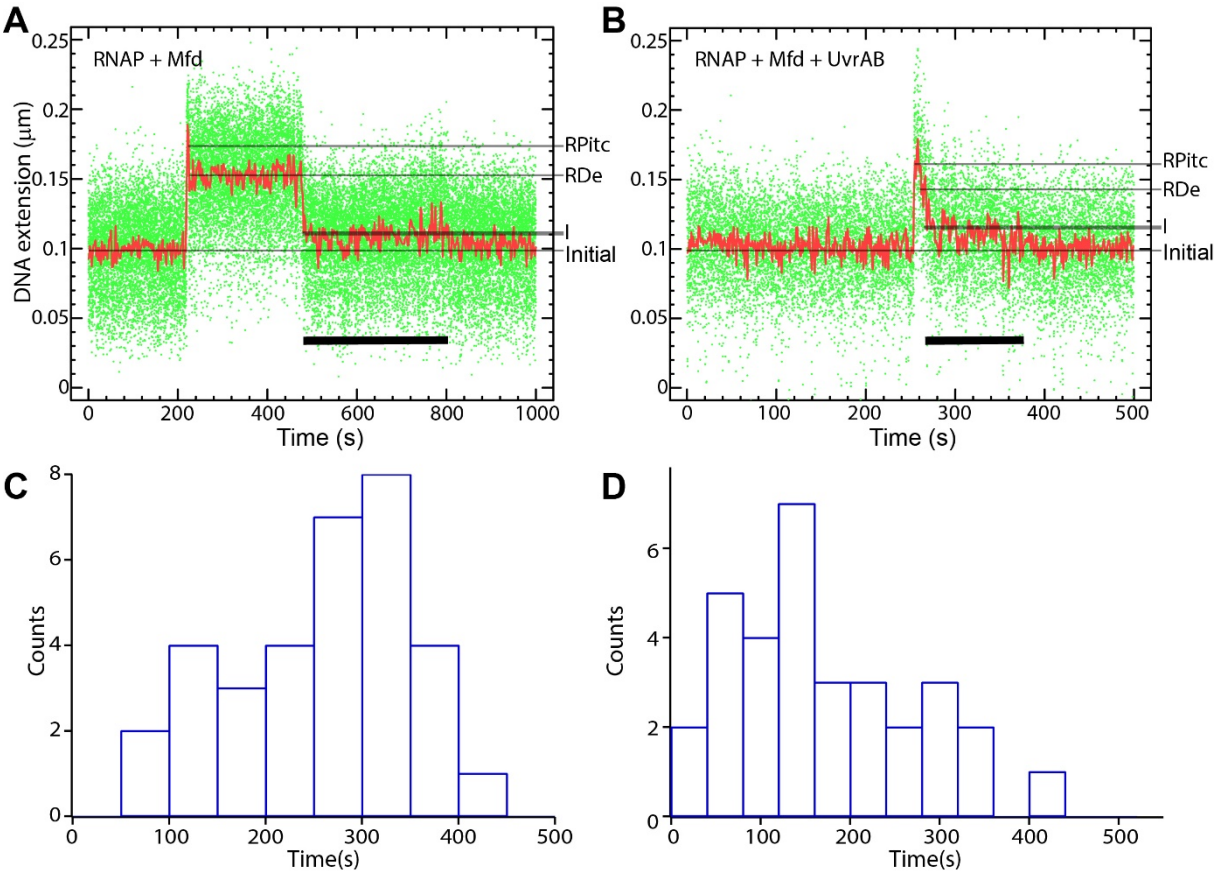

Extended Data Figure 4

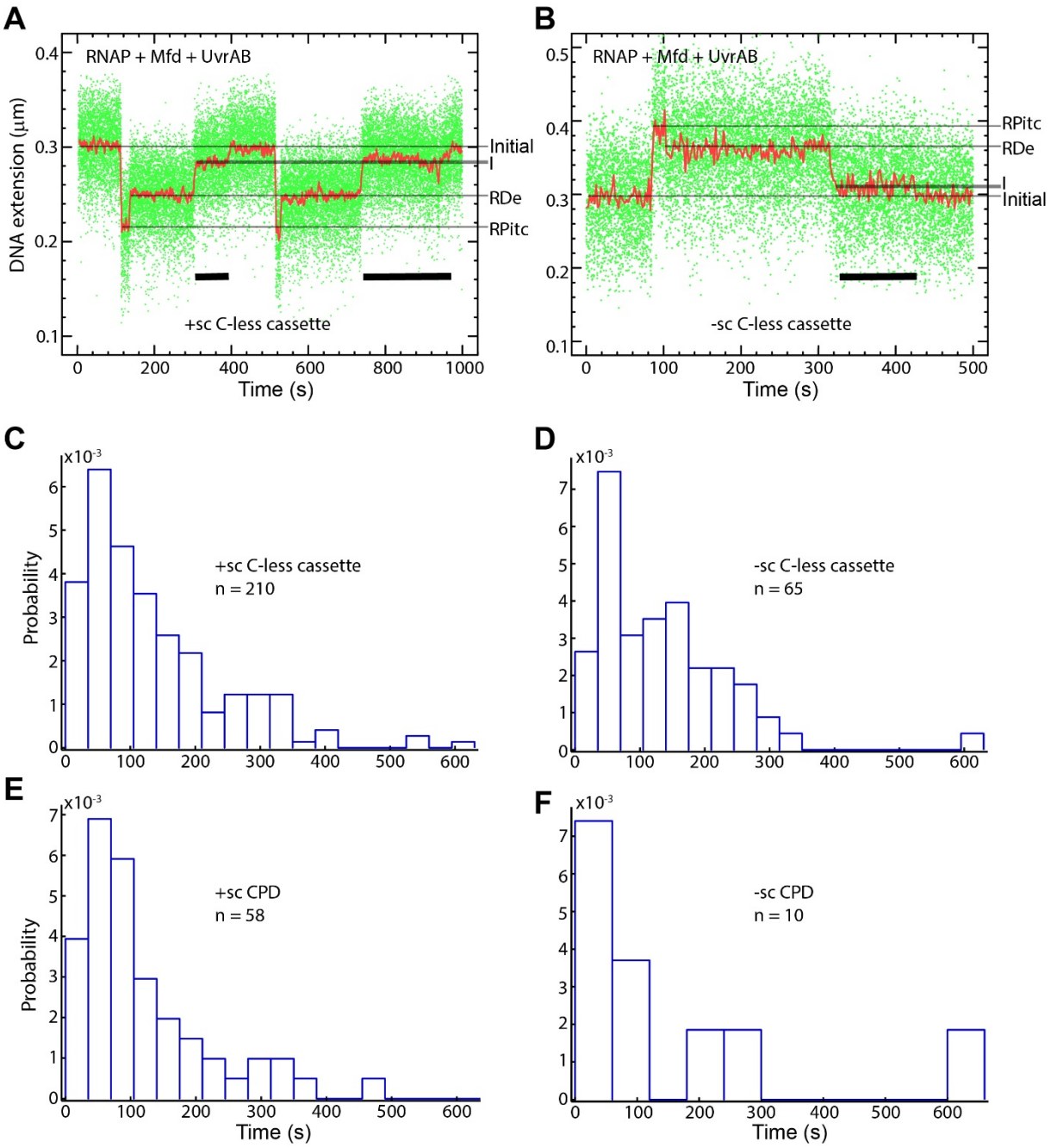

Extended Data Figure 5

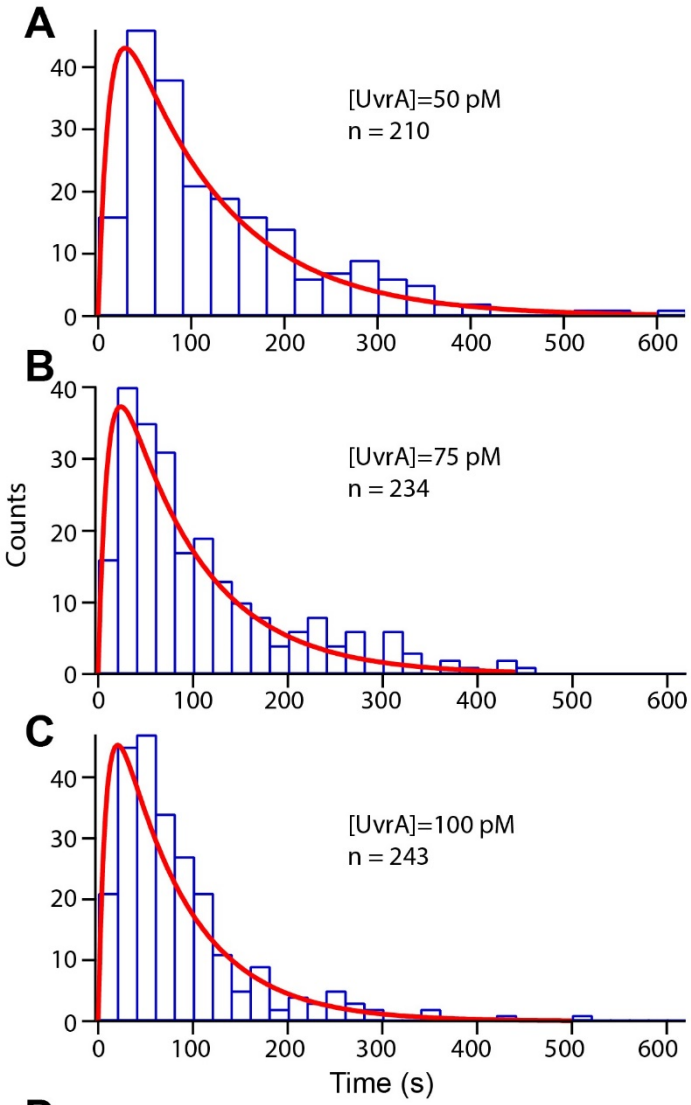

D

Supercoiling	DNA	[UvrA] (pM)	Mean lifetime of inter-mediate(s)	Number of events	σ	S.E.M.(s)
Positive supercoiling	C-less cassette	50	132	210	108	7
		75	110	234	94	6
		100	86	243	75	5
	CPD cassette	50	141	58	153	20
		100	85.7	52	70.7	9.8
Negative supercoiling	C-less cassette	50	132	65	103	12.7
	CPD cassette	50	157	10	205	64.8

Extended Data Figure 6

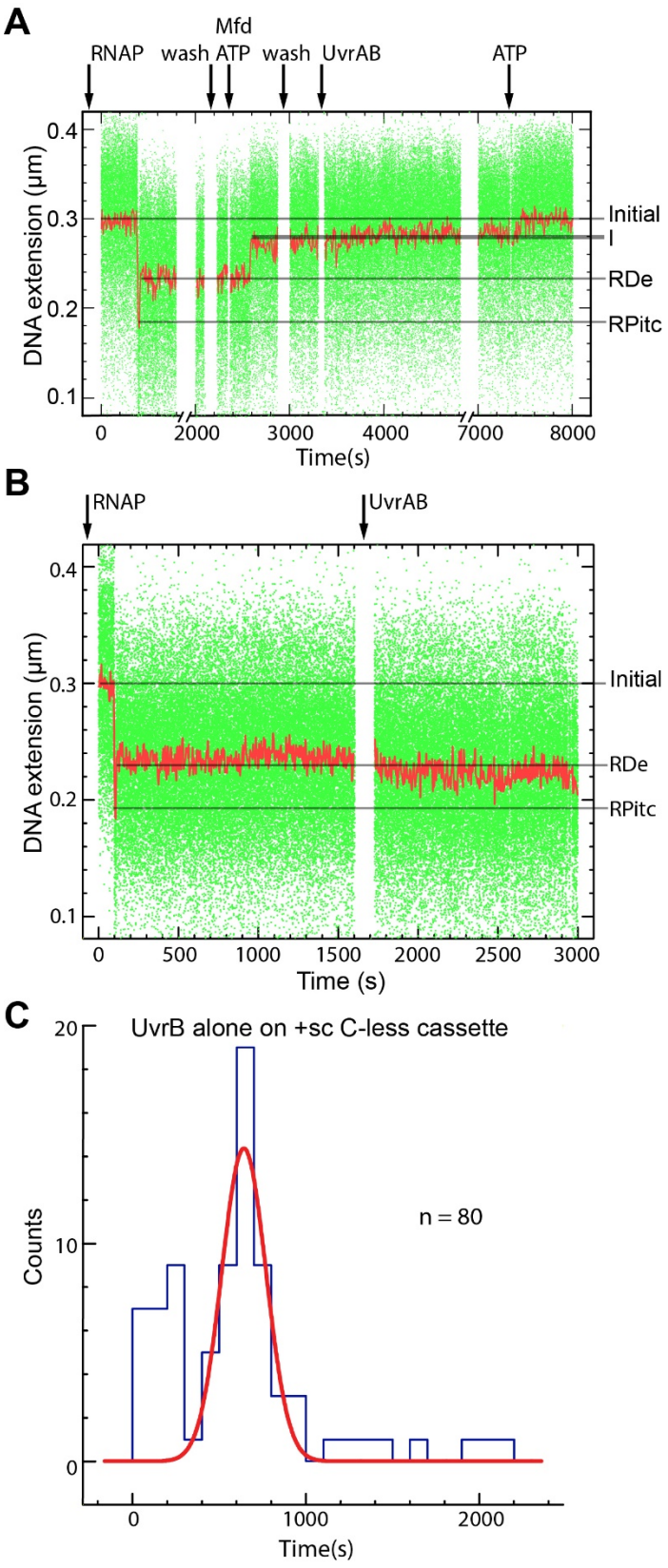

Extended Data Figure 7

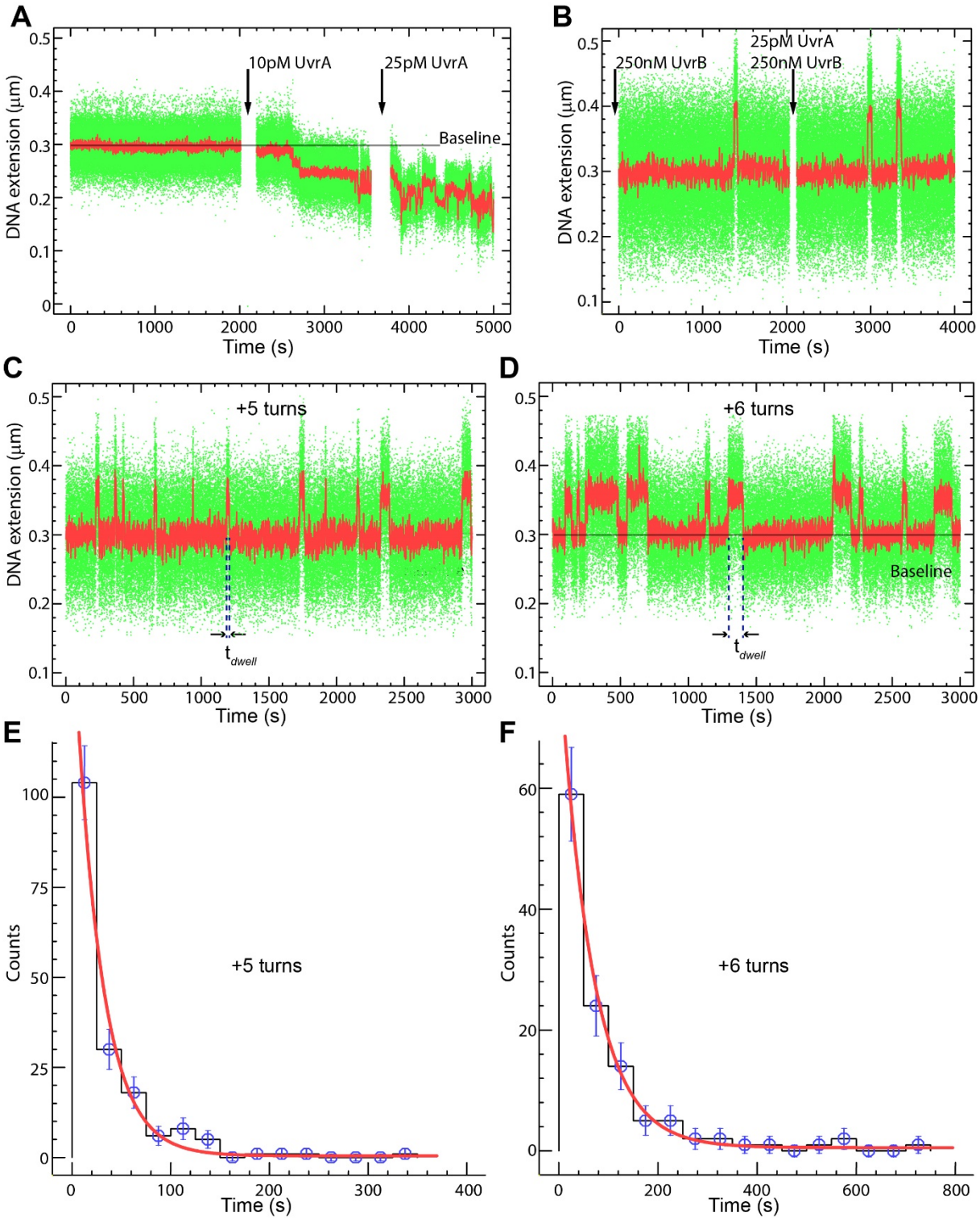

Extended Data Figure 8

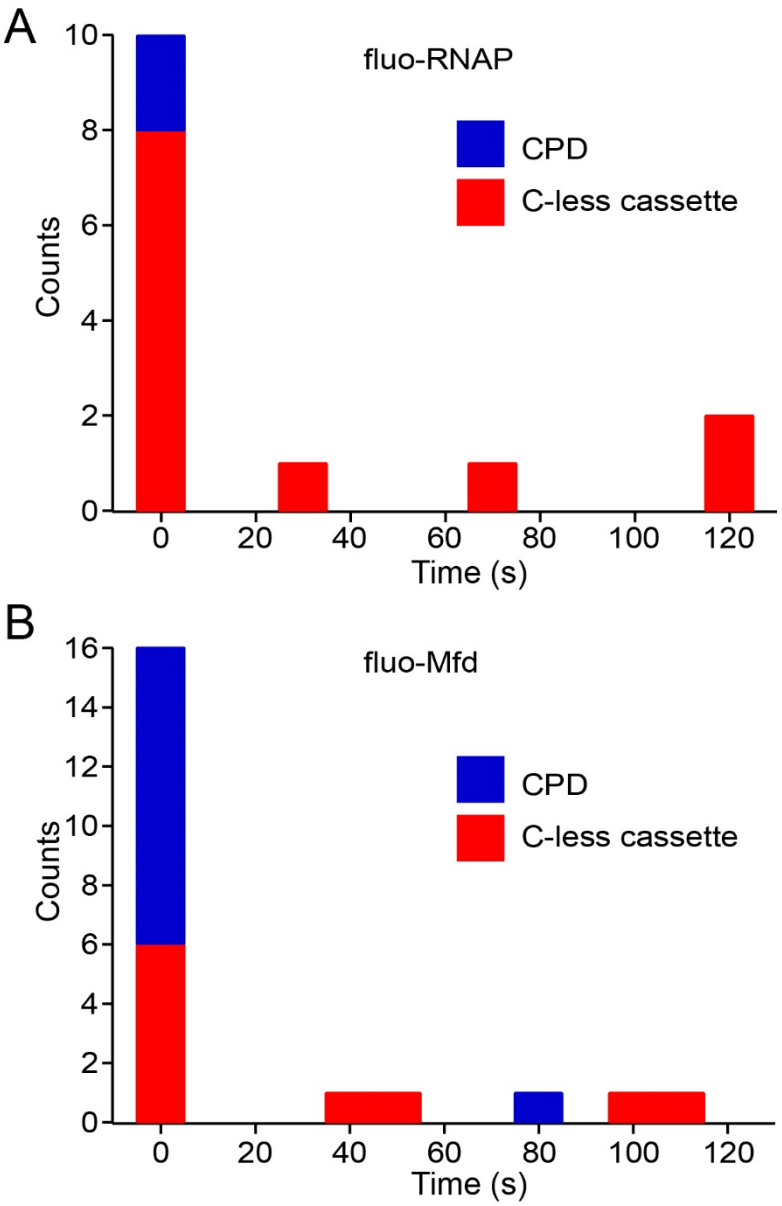

Extended Data Figure 9

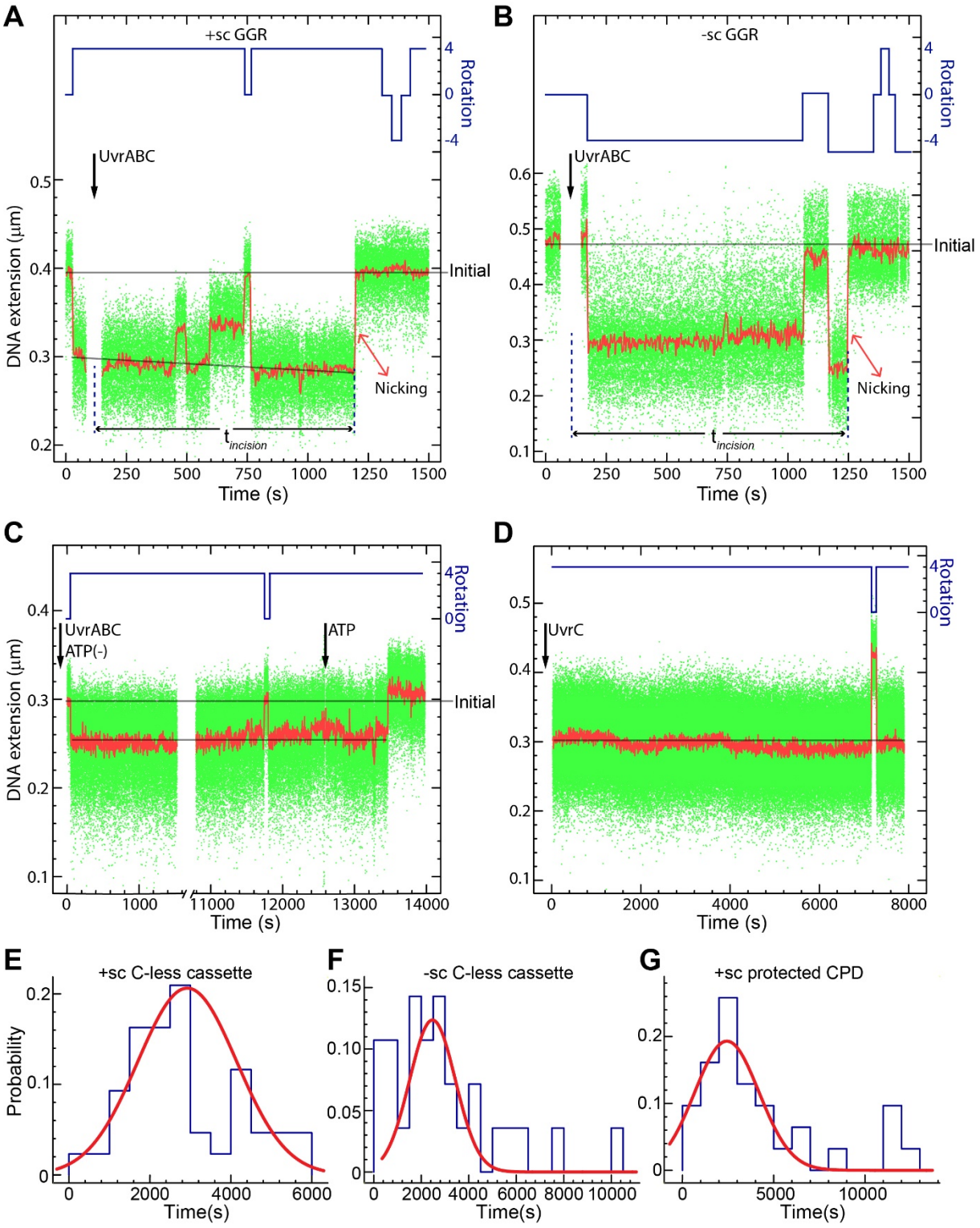

Extended Data Figure 10